THE JOURNAL OF PHYSICAL CHEMISTRY C

Article

pubs.acs.org/JPCC

Fluorescence and Scattering Dual-Mode Multiplexed Imaging with Gold−Silver Alloy Core Silica Shell Nanoparticles

Siyu Tu,[†] David Rioux,[†] Josée Perreault,[‡] Danny Brouard,*[,‡] and Michel Meunier*[,†]

[†]Department of Engineering Physics, Polytechnique Montréal, Montréal, Québec QC H3T 1J4, Canada

[‡]Research and Development, Héma-Québec, Québec, Québec G1V 5C3, Canada

Supporting Information

ABSTRACT: Gold−silver alloy core silica shell nanoparticles ($Au/Ag@SiO_2$ NPs) with fully accordable photophysical properties were developed and used as contrast agent for multiplexed cell-imaging applications. Using a seed growth strategy, these nanoparticular labels can be designed to suit specific experimental needs and be clearly identified based on their distinctive combination of scattering and fluorescence colors. In this Article, the multiplexed cell-imaging capabilities of $Au/Ag@SiO_2$ NPs are presented using four different combinations of core composition and fluorescence colors. In a proof of concept experiment, 86% of total nanoparticles were correctly identified by an optical microscope with a system offering fluorescence and darkfield detection capabilities. This multiplatform identification strategy was successfully applied for the detection of four different nanoparticular architectures in cell-imaging experiments.

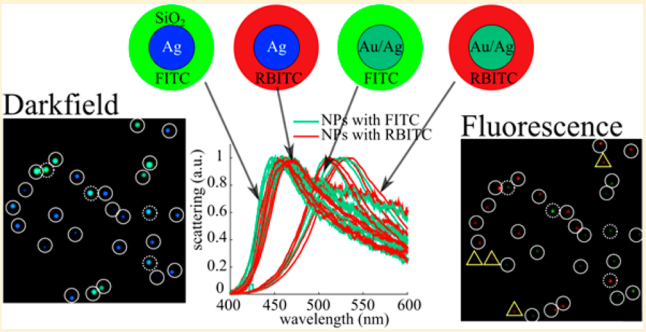

INTRODUCTION

During the last few decades, nanotechnology has emerged as one promising research field leading to the development of multiple nanoparticular architectures currently used in an extended range of imaging, sensing, and catalyst applications, among many others.[1−8] Metallic nanoparticles (NPs) have attracted much attention because of their outstanding photophysical properties highlighted in various biomedical applications.[9−13] In this Article, the plasmonic properties of greatly uniform gold−silver alloy NPs were exploited for the design of superluminescent contrast agents for multiplexed analysis in cell-sorting and cell-imaging applications. Cell analysis is an integral part of biochemical experiments, and numerous techniques are available to obtain relevant information on cell identity, structure, function, or current state.[14−20] Plentiful applications involve protein quantification, structural staining, and, for the purpose of this work, immunofluorescence labeling, which takes advantage of the antibody−antigen recognition reaction. The use of fluorophore-labeled antibodies to highlight specific intra- or extracellular antigens has led to the development of cell characterization assays for fluorescence microscopy and flow cytometry applications. In the case of studies dealing with weakly expressed antigens or rare-events detection issues, the use of highly luminescent and time-stable fluorophores is recommended to maximize detectability and the signal-to-background ratio. Moreover, most cell-characterization experiments involve the use of multiple cell-labeling moieties together to obtain various information on cell populations simultaneously. Multiplexed analysis is limited, however, by the ability of the sensing system to isolate each cell label in a single detection channel with minimal crosstalk. In the case of fluorescence-based detection techniques, for example, one must consider the use of fluorophores with narrow emission bands to minimize spectral overlap leading to experimental issues and complex results interpretation.

Fluorescent dyes are commonly used as labels, but they tend to suffer from photobleaching and large excitation and emission bandwidths,[21,22] thus limiting their use to very short observation time in the case of microscopy experiments or to fewer detection channels (<7 colors)[23] for flow cytometry applications. The use of quantum dots (QDs) for cell labeling has emerged as an alternative strategy for multiplexed analysis assays because of their narrow and tunable emission band.[23−25] However, the fluorescence intermittency (blinking) and their potential toxicity limit their use as reliable contrast agents for biological applications.[21,23,26,27] Plasmonic nanomaterials, more especially gold or silver NPs (AuNPs and AgNPs), have been applied to a wide range of applications including labels for cell-tagging applications.[28,29] Among others, NPs used as contrast agents were previously reported for optical, electronic, X-ray, or magnetic resonance image observations[30−32] and, more interestingly, as fluorescence quenchers or signal enhancers within a variety of fluorescent core−shell architectures.[33−35] Recently, multiple research groups have shown interest in the unique photophysical properties of plasmonic NPs for multiplexed analysis.[9,12,36,37] For example, the scattering band

Received: November 28, 2016
Revised: March 17, 2017
Published: March 29, 2017

DOI: 10.1021/acs.jpcc.6b11954
J. Phys. Chem. C 2017, 121, 8944−8951

of plasmonic active NPs can be adjusted by the modification of their size, composition, or geometrical shape.[38−40] Unlike fluorescence or quantum dots luminescence, scattering does not present any kind of dark state or blinking and is not subject to photobleaching, allowing extended observation periods under low-intensity illumination, thus improving the signal-to-background ratio for better detection contrast. For example, Bergeron et al. reported the use of a reflected-light microscope dedicated to plasmonic imaging for multiplexed analysis of cancer cells using Au and Ag NPs together with Au nanorods as contrast agents.[21] This study has motivated the development of a NP system offering the fully accordable plasmonic and fluorescence properties for improved multiplexed possibilities. Recently, our group has proposed a gold−silver alloy NP (Au/AgNPs) synthesis based on a seed-growth approach offering remarkable features in terms of size and composition adjustability.[40] Au/AgNPs with different size diameters generating predetermined scattering colors were successfully prepared, observed, and identified under darkfield (DF) microscopy.[12]

The presence of metallic structures near fluorescent dyes is known to improve their photophysical properties. Noble metals such as gold and silver are frequently being used to increase fluorescence signals due to near-field photophysical interactions, a phenomenon called metal-enhanced fluorescence (MEF).[41−43] When there is MEF, the fluorophore excitation and emission rates increase as its excited state lifetime reduces, which leads to an apparent increase of quantum yield and photostability. Nanoparticular core−shell architectures with dye-doped silica shells have been designed to exploit the advantages of MEF over commonly used fluorescent molecules.[33,34,44−46] Core−shell NPs can be ingeniously designed to position fluorophore molecules at a precise distance from the NP surface to maximize fluorescence and avoid metallic quenching.[47] Moreover, the presence of a silica-shell around the metallic core improves the NP colloidal stability[48] and maximizes the surface-modification possibilities, thanks to the now well-known silica processing chemistry.[49]

In this Article, we propose alloy-core and fluorescent silica-shell NPs (Figure 1) as contrast agents in a multiplatform

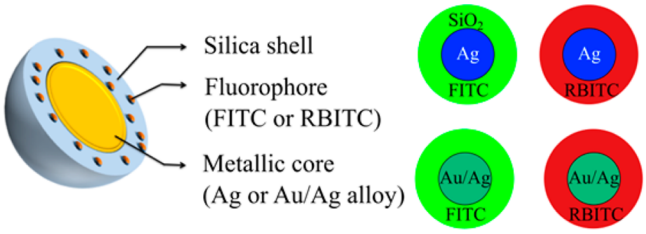

Figure 1. Schematic of alloy-core and fluorophores embedded silica-shell nanoparticles with the four types of core−shell NPs used as contrast agent in this work.

detection strategy for improved multiplex detection capabilities. The idea is to develop an accordable NP system exhibiting highly controlled fluorescence and plasmonic scattering features. In a proof-of-concept study, silver-core and silica-shell NPs (Ag@SiO_2) along with 50/50 Au/Ag alloy core silica shell NPs (Au/Ag@SiO_2) were prepared. Using a simple chemistry reaction, fluorophores molecules (fluorescein isothiocyanate (FITC) or rhodamine B isothiocyanate (RBITC)) were covalently incorporated inside the silica shell (Table 1), resulting in four different color combinations of contrast agents that can be differentiated using fluorescence and darkfield microscopy.

Table 1. Four Types of Core−Shell NPs As Contrast Agent[a]

core	AgNPs		Au/AgNPs	
fluorophore	FITC	RBITC	FITC	RBITC
NPs	Ag@ SiO_2+FITC	Ag@ SiO_2+FITC	Au/Ag@ SiO_2+FITC	Au/Ag@ SiO_2+RBITC

[a]Four types of NPs synthesized with Ag and 50/50 Au/Ag alloy core coated with a fluorescent silica shell (FITC or RBITC).

EXPERIMENTAL METHODS

Materials. Gold−silver alloy NPs with different sizes and compositions were fabricated by a successive seeded growth method of alloy on initial ∼15 nm diameter Au seeds.[40] $HAuCl_4$, $AgNO_3$, and trisodium citrate (Na_3Cit) were purchased from Sigma-Aldrich. Silver NPs used in this study, 0.02 mg/mL (∼70 nm), were received from nanoComposix (no. AGCN70). For the fluorescent precursor synthesis, anhydrous *N*,*N*-dimethylformamide (DMF, Aldrich no. 68-12-2), triethylamine (Aldrich), 3-(aminopropyl)triethoxysilane (APS, Aldrich no. 919-30-2), fluorescein isothiocyanate (FITC, Aldrich no. 27072-45-3), Rhodamine B isothiocyanate (RBITC, Aldrich no. 36877-69-7), and CF 647 dye (Aldrich no. SCJ4600048) were used as received. For the silica shell coating preparation, tetraethyl orthosilicate (TEOS, Aldrich no. 78-10-4), 28−30% $NH_3{\cdot}H_2O$ (Aldrich no. 7664-41-7), and anhydrous ethanol (EtOH) were used as reagent, catalyst, and dispersion media, respectively. Eighteen MΩ deionized water was obtained from a EMD Millipore water purifier.

Preparation of Fluorescent Precursors. FITC-APS and RBITC-APS were prepared following a similar protocol.[58] They were prepared in DMF with triethylamine as a catalyst. Typically 2.2 mg (5.7 μmol) of FITC was mixed with 150 μL of DMF, 2 μL of triethylamine, and 2 μL of APS in a light-proof tube in continuous agitation at 50 °C for 3 h. The solution was diluted in 13.5 mL of EtOH, resulting in a fluorophore solution at 420 μM. Similarly, 3 mg of RBITC was mixed with 4 μL of APS in 150 μL of DMF and 2 μL of triethylamine with all other reagents and reaction conditions being the same.

Preparation of Fluorescent AuAg@SiO_2 NPs. Eighty nm 50/50 Au/Ag and 74 nm Ag NPs were used as the core. For the fluorescent silica shell synthesis, 4 mL of a 50/50 Au/Ag alloy NP aqueous solution at ∼5×10^9 NPs/mL was added directly to 12 mL of anhydrous EtOH under continuous stirring. Then, 1.2 μL of TEOS and 625 μL of 30% ammonia solution were added. A small volume of the fluorescent silica precursor (50 μL for FITC per example) was added directly to the nanoparticles solution 30 min after the start of the silica-coating process to reduce the amount of fluorophore quenched because of their close proximity to the metal core. After a 24 h reaction period, the fluorescent core−shell nanoparticles were clean and dispersed in ethanol and stored at 4 °C away from light until their use.

Nanoparticle Characterization. UV−visible experiments were carried out on an Epoch Microplate spectrometer and used to study the plasmonic band evolution and evaluate the colloidal stability of nanoparticles at every step during synthesis. The steady-state fluorescence measurements were realized with a Varian Cary Eclipse. The structure of each nanoparticle

DOI: 10.1021/acs.jpcc.6b11954
J. Phys. Chem. C 2017, 121, 8944−8951

sample was defined by transmission electron microscopy (TEM, JEOL 2100), and the data were used to generate size distributions and to confirm core−shell morphology. Copper grids (Pacific grid tech, Cu-400CN) were dipped into diluted NPs ethanol solution and air-dried before TEM analysis.

DF and fluorescent microscopy images were acquired with an Eclipse Ti microscope (Nikon) equipped with a 100× oil-immersion objective (numerical aperture (NA) 0.5−1.3, Nikon) with with a 4.2 megapixel color CMOS camera (xiQ, 2048 × 2048 pixels) or a QIclick CCD camera (Qimaging, 1392 × 1040 pixels) for detection and imaging. Two light sources were available, a 100 W halogen lamp (Nikon) and the Intensilight Epi-fluorescence Illuminator from Nikon for DF and fluorescence applications, respectively. FITC (Thorlabs, MDF-FITC, excitation filters/emission filters: 475 ± 35 nm/530 ± 43 nm, dichroic: 470−490 nm/508−675 nm) and RBITC (Nikon, TRITC/Cy3 long pass filter set, excitation filters/emission filters: 540 ± 25 nm/605 ± 55 nm long pass, dichroic: 565 nm) filters were used for fluorescence measurements. The sample preparation method for microscopy experiments was developed to obtain a final NP concentration of ∼1 NP/μm^2 in the instrument field of view. The hyperspectral images were acquired using an imaging spectrograph (Shamrock 750, Andor Technology) equipped with an EMCCD camera (Newton 971, 1600 × 400 pixels, Andor Technology) and a 150 lines per mm grating providing a 242 nm bandpass.

RESULTS AND DISCUSSION

Structural and Composition Characterization. Figure 2 shows transmission electron microscopy (TEM) images of pure Ag and 50/50 Au/AgNPs before and after the silica shell formation. The silica shell thicknesses are ∼12 and ∼27 nm for the alloy and silver core−shell NPs, respectively. TEM image analysis confirms that there is a decrease in the size of the silver core during the synthesis of Ag@SiO_2 NPs (see Figure 2e). The initial mean diameter of Ag NPs was 70 ± 8 nm and decreased to 55 ± 7 nm after the fluorescent silica-coating preparation (Figure 2f). On the other end, the mean diameter of alloy NPs was not affected by the silica-coating synthesis and remained constant at 84 ± 9 nm (Figure 2c). The size reduction for Ag NPs is probably caused by an etching effect during the tetraethyl orthosilicate (TEOS) polymerization process catalyzed by ammonia. Indeed, Ung and Liz-marza[50] have reported a similar effect and attribute the etching effect to the oxidization of silver in the presence of ammonia. The same group has also studied the effect of ammonia on small (<30 nm) bimetallic NPs with 25/75, 50/50, 75/25 Au/Ag compositions. They showed that the etching effect is far less severe for Au rich and 50/50 Au/Ag NPs than Ag rich NPs,[51] in agreement with the results of Figure 2.

To evaluate the core-etching effect of the silica-coating synthesis for Au/AgNPs, we prepared two types of alloy NPs having similar mean diameters (59 ± 5 and 61 ± 8 nm) with different Au/Ag core-composition ratios (10/90 and 50/50). A silica shell was grown on both alloy NPs using the same experimental conditions. Post-synthesis TEM image analysis confirmed that the etching effect was more important for silver-rich alloy NPs. The TEM image-analysis results (Figure 3c and g) show a reduction of the core diameter for 10/90 Au/Ag@SiO_2 (59 ± 5 to 43 ± 4 nm) while there was no significant change for 50/50 Au/Ag@SiO_2. The corresponding energy-dispersive X-ray spectroscopy (EDS) results (Figure 3d and h)

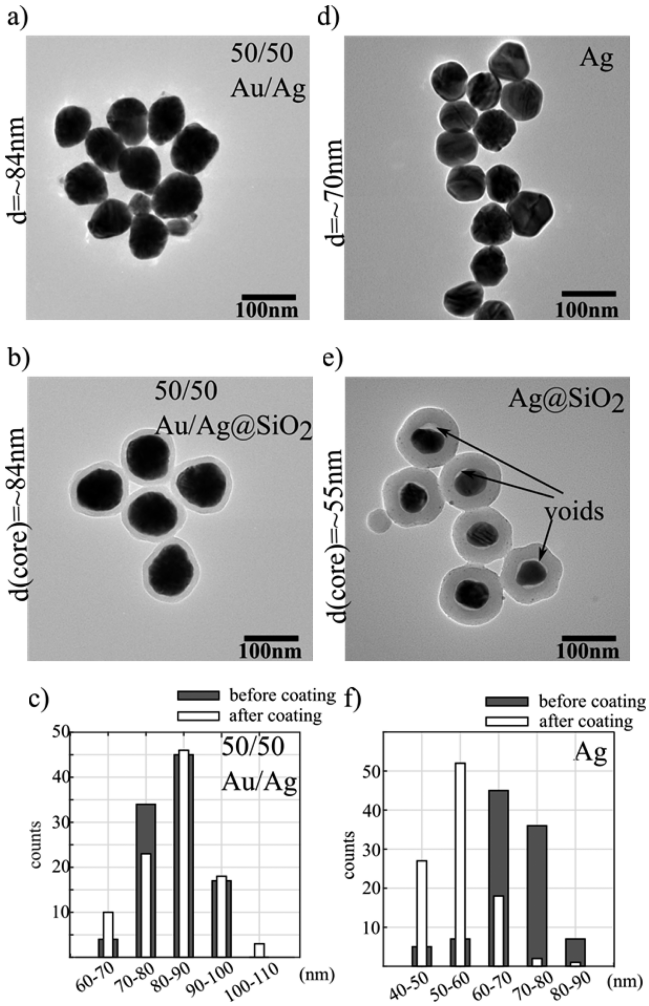

Figure 2. TEM images before and after silica coating for (a, b) 50/50 Au/AgNPs and (d, e) pure Ag NPs along with (c, f) their respective size distribution. (e) TEM images for Ag@SiO_2 NPs clearly shows voids near Ag cores resulting from etching during the coating process.

show a significant 30% reduction in the silver composition for 10/90 Au/Ag@SiO_2 after the silica shell synthesis compared to only ∼5% for 50/50 Au/Ag@SiO_2. These results confirm that Au/AgNPs with higher gold ratios are less prone to the core-etching process, which can take place during the silica-coating reaction. The mechanism of Au protecting NP from etching is not entirely clear. However, as proposed by Rodríguez-González et al.,[51] gold atoms could rearrange and would have a protecting effect on silver, preventing further etching during the silica-core synthesis because they are less affected by ammonia. From AgNPs, 10/90 Au/Ag NPs and 50/50 Au/Ag NPs, the above results (Figures 2 and 3) show that, during the silica-coating process with ammonia as catalyst, the 50/50 Au/Ag alloy NPs endure the least size reduction phenomenon. Therefore, the higher the gold ratio is for the starting NPs, the easier the silica layer can be generated around the core without any significant core size reduction.

Optical Characterization. Characterization of the photophysical properties for gold, silver, or alloy nanoparticles were compared to their corresponding theoretical extinction spectra obtained using Mie Theory calculations.[52] The UV−visible spectra for Ag@SiO_2 and 50/50 Au/Ag@SiO_2 measured before and after the silica-coating process are presented in Figure 4

DOI: 10.1021/acs.jpcc.6b11954
J. Phys. Chem. C 2017, 121, 8944−8951

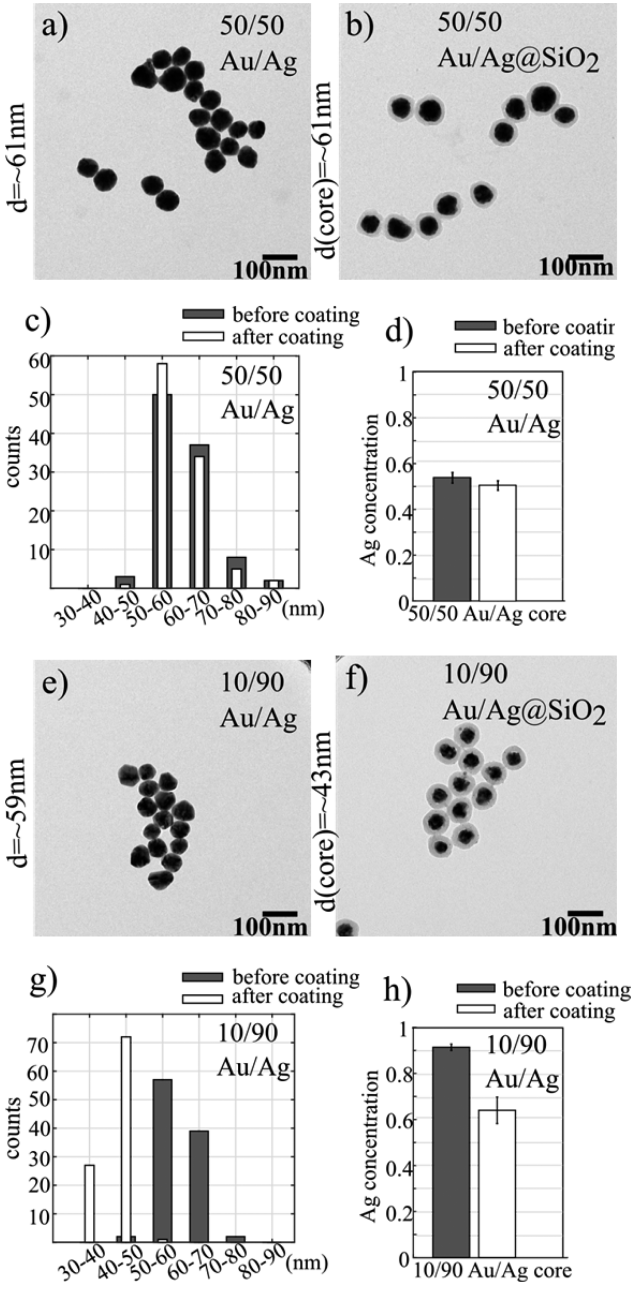

Figure 3. TEM images for (a) 61 ± 8 nm 50/50 Au/AgNPs and (e) 59 ± 5 nm 10/90 Au/AgNPs and after coating with silica shell (b) 50/50 Au/Ag@SiO_2 and (f) 10/90 Au/Ag@SiO_2. The respective NP diameter distributions are shown in (c) and (g). Silver concentration bar graph are presented for (d) 50/50 Au/AgNPs and (h) 10/90 Au/AgNPs before and after silica coating based on energy-dispersive spectroscopy (EDS) examination of 5 individual NPs.

and can be compared to their theoretically calculated ones for both FITC and RBITC silica-embedded fluorophores. The absorption of both FITC and RBITC can hardly be observed because of their relatively low absorption intensities compared to the extinction of metallic NPs. The dielectric function for Au/AgNPs was taken from Rioux et al.,[53] and the refractive index for the silica shell was computed using the dispersion equation from Malitson.[54] Core diameters and silica-shell thicknesses considered for calculations were evaluated by TEM image analysis (details in Supporting Information).

As expected, a red-shift of the plasmonics band is observed for the 50/50 alloy NPs after the silica-coating process (Figure 4a). The ~15 nm red-shifts recorded for both nanoparticles were confirmed by Mie calculations (Figure 4a-i).[55] An unexpected smaller (~3 nm) red-shift was measured for Ag@SiO_2+RBITC NPs and even more surprisingly, a ~6 nm blue shift was observed for Ag@SiO_2+FITC NPs even if their corresponding smaller core size were considered in the calculations. The experimental results for Ag@SiO_2 were significantly different from the theoretically expected ones based on nanoparticular core−shell architectures. TEM observations of Ag@SiO_2+RBITC and +FITC samples indicated the presence of voids between the core and the shell (Figure 2 e), which have direct impacts on the position of the NPs plasmonics band. The silver-core-etching phenomenon may originate from the presence of ammonia during the silica-coating process.[56] Consideration of smaller core size diameters (Figures 2f and 3g) in the calculations could not explain the results observed as there was still a ~10 nm discrepancy with the experimental measures (Figure 4b-i and b-ii). Therefore, reconsideration of the nanoparticular architecture was realized in order to take into account the presence of a 5 nm thick space filled with the NP suspension medium. Using this modified model (see parameters used in Supporting Information), the calculated spectra for Ag@SiO_2+RBITC and +FITC were virtually identical to their counterpart measured experimentally (Figure 4b-ii and b-iii).

Fluorescence characterization for Ag@SiO_2 and 50/50 Au/Ag@SiO_2 NPs are detailed in Supporting Information for FITC- and RBITC-embedded core−shell NPs. The MEF factor was measured for Ag@SiO_2 NPs with RBITC by comparing the maximum fluorescence intensity of a Ag@SiO_2 RBITC solution before and after a complete core-etching process using a 250 mM sodium chloride solution. A MEF factor value of 4 was calculated for the Ag@SiO_2+RBITC (see Supporting Information). There are many studies demonstrating the impact of the fluorophore−metal distance on fluorescence intensity and MEF factor.[42,57] The core−shell nanoparticle synthesis has been developed to obtain the maximum fluorescence intensity from the nanoparticle knowing that there is a non-negligible fraction of fluorophores positioned at the close distance from the core that could experience metal quenching and leading to an underestimate of the MEF factor.

Multiplexed Imaging. The principal objective of this Article is to present a multiplatform detection approach exploiting the remarkable photophysical properties of alloy-core and fluorescent silica-shell nanoparticles for multiplexed imaging applications. The strategy is based on the use of spectrally distinguishable nanostructures offering multiple combinations of scattering and fluorescence colors. In this proof-of-concept study, four different color-coded NPs were mixed together and sampled on a glass slide. Single-particle identification was accomplished by acquiring the scattering spectra and the fluorescence properties of each nanoparticle. Ag@SiO_2 and 50/50 Au/Ag@SiO_2 appear blue and green under darkfield microscopy, respectively. Their specific color is attributed to the position and shape of their plasmonics band, which have a maximum at ~450 nm for silver core NPs and ~520 nm for 50/50 Au/AgNPs. A spectrometer was positioned on the detection path of the optical microscope used in this study in order to acquire the individual scattering spectrum of each nanoparticles. Attribution of the core compositions was realized using each nanoparticle's maximum scattering value.

DOI: 10.1021/acs.jpcc.6b11954
J. Phys. Chem. C 2017, 121, 8944−8951

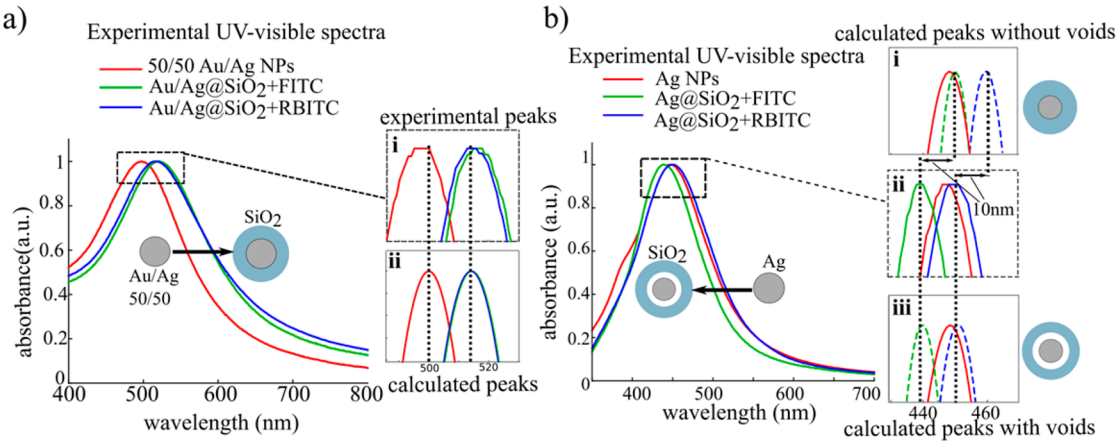

Figure 4. Presentation of the experimental and calculated UV−visible spectra for (a) 50/50 Au/AgNPs and (b) Ag NPs before and after the silica shell coating process (with FITC and RIBTC). A ∼15 nm red-shift of the plasmonics band maximum was observed between 50/50 Au/Ag NPs and 50/50 Au/Ag@SiO_2 independently of the fluorophore embedded in the silica shell. The same red-shift was smaller (∼3 nm) for Ag@SiO_2+RBITC, and a 6 nm blue-shift was measured for Ag@SiO_2+FITC. Calculated UV−visible spectra of 50/50 Au/AgNPs (a-ii) and Ag NPs (b-i, b-iii) before and after silica coating are aligned to the experiment peaks. For both FITC- and RBITC-incorporated Ag@SiO_2 NPs, the blue-shift of the plasmonics band results from the presence of a void layer between the silver core and the silica shell (b-iii, a 5 nm void was used for this calculation, estimated from TEM images). The schematics show the nanoparticle geometries considered for the calculations.

Globally, scattering spectra of 28 particles were recorded as shown in Figure 5c and d. On the other end, fluorescence

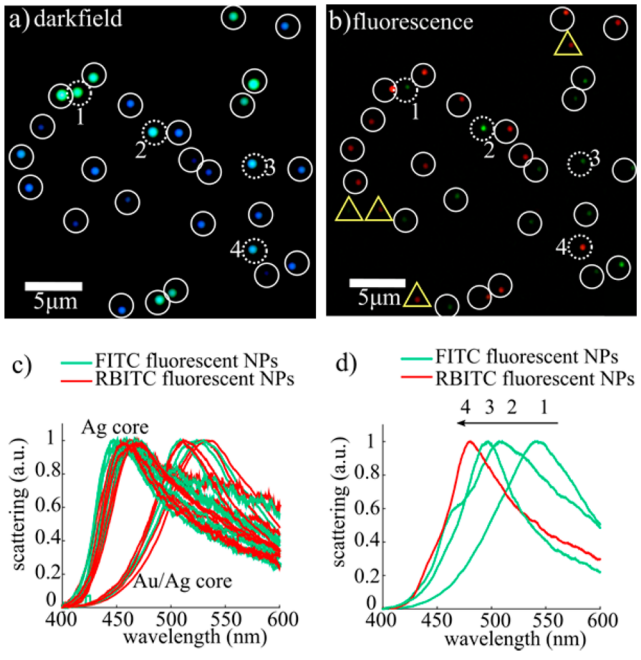

Figure 5. (a) Darkfield and (b) fluorescence microscopy images of a Ag@SiO_2 and 50/50 Au/Ag@SiO_2 mixture. (c) Scattering light identification of each identifiable nanoparticle and presentation of the scattering spectra for (d) four specific NPs identified by dashed circles in figures (a). Fluorescence signal from NPs identified by yellow triangles in (b) do not show corresponding scattering signal in (a).

identification was performed by measuring the signal intensities in each detection channel for all nanoparticles (FITC and RBITC) (Figure 5b). Using optical filter sets specific to each fluorophore, detection thresholds were fixed at three times the standard deviation (pixel to pixel) over the average intensity recorded for a blank sample (nanoparticle-free). Figure 5c shows that 24 of 28 NP cores were correctly identified by their scattering maximum, resulting in a 86% core-composition differentiation capability. Four NPs, noted as dashed circles 1, 2, 3, and 4 in Figure 5a and b, were not correctly identified because of their higher scattering intensities, broader scattering spectra, and more ambiguous peak position compared to the other NPs (Figure 5d), probably as a result of clusters formation. Finally, we observed several isolated fluorescence spots without any scattering signals (noted in yellow triangles). These NPs might be either core-free silica NPs or fluorescent silica fragments that do not produce any coloration under darkfield microscopy.

We assessed the performances of fluorescent Au/Ag@SiO_2 as contrast agents for cell-imaging applications. A 1:1 mixture of Ag@SiO_2 and 50/50 Au/Ag@SiO_2 NPs with either a FITC (Au/Ag@SiO_2+FITC) or a RBITC (Au/Ag@SiO_2+RBITC) fluorescent silica shell was added to a dead retina cells sample (ARPE-19). The latter was observed by darkfield and fluorescence microscopy, and a representative image of the probed area is presented in Figure 6. Stronger photoluminescent spots were attributed to NP clusters, which is a hypothesis confirmed by darkfield microscopy. Eight circled nanoparticles were characterized and clearly identified by their respective scattering and fluorescence properties (Figure 6c−e). This experiment demonstrates how the fully accordable photophysical properties of alloy-core and silica-shell nanoparticles can be exploited in a multiplatform detection strategy for cell-imaging applications with multiplexed analysis capabilities.

Reflected light microscopy offers exceptional detection contrast when using NPs as cell labels for imaging applications in highly diffusing media.[12] Fluorescent Au/Ag@SiO_2 were added to a dead retina cells sample, and the latter was observed by fluorescence, darkfield, and reflected-light microscopy. Each image was compared to a nanoparticle-free sample (Figure 7). Experimental results confirm the high potential of the use of alloy-core silica-shell NPs as effective contrast agents for all three modes of optical microscopy. The scattering light for cells is stronger under darkfield microscopy, making nanoparticle detection and identification more complicated. Rather, the same scattering signal is significantly lower for reflected light

DOI: 10.1021/acs.jpcc.6b11954
J. Phys. Chem. C 2017, 121, 8944−8951

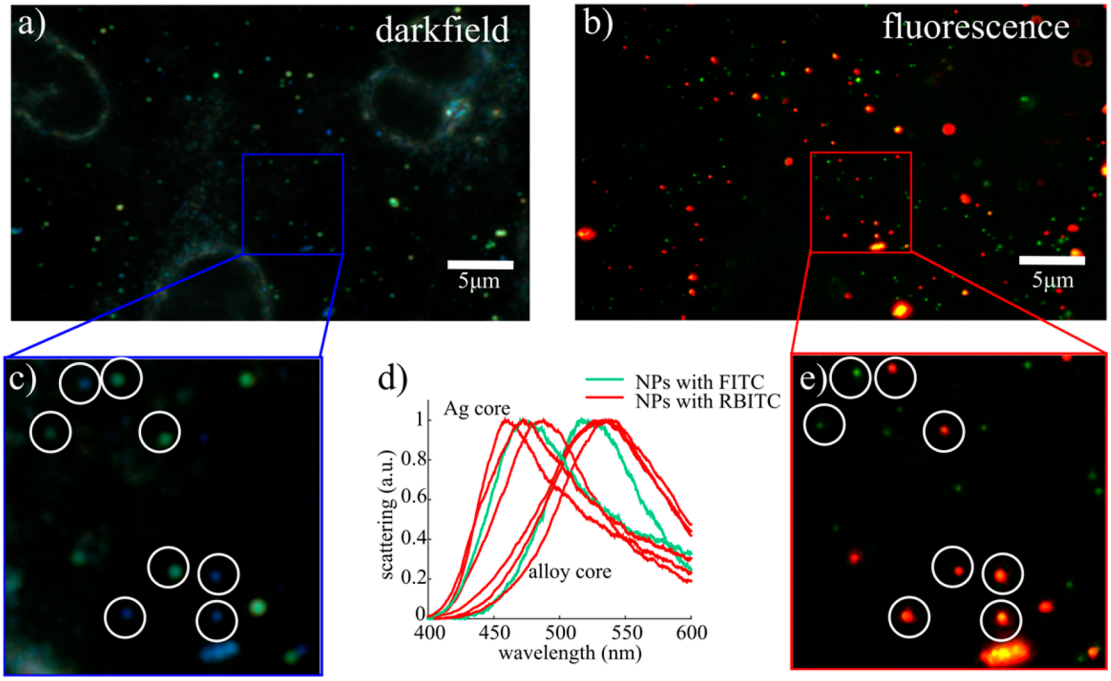

Figure 6. (a) Darkfield and (b) fluorescence images of a retinal cell sample (ARPE-19) in the presence of a nanoparticles mixture with their respective close-up views (c and e). (d) Characterization of the scattering and fluorescence properties for eight nanoparticles identified by circles in (c) and (e). The four types of color-coded nanoparticles were identified by their scattering spectra and fluorescence properties.

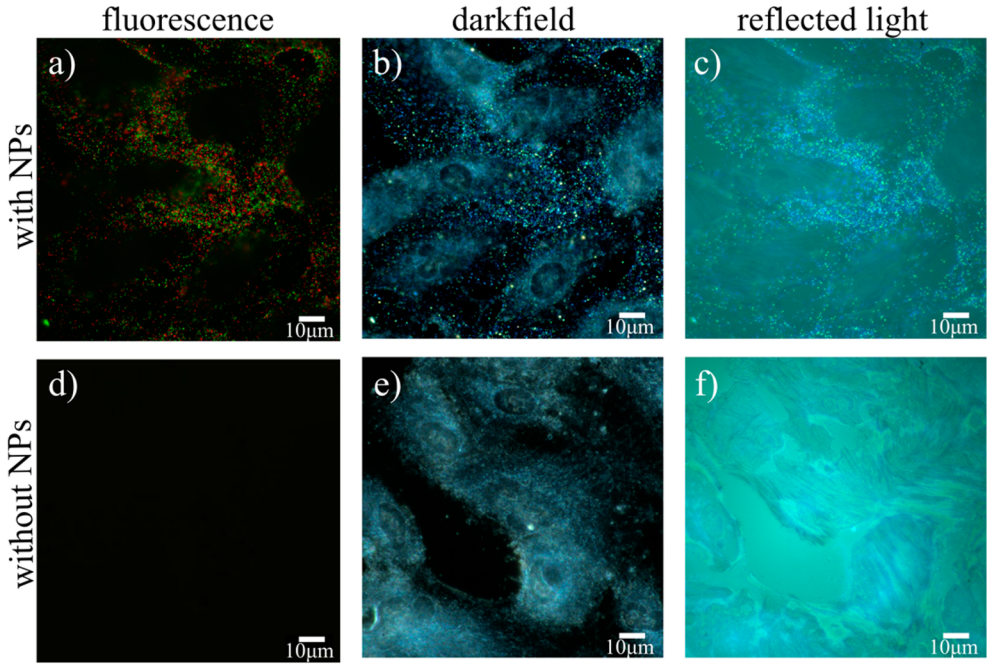

Figure 7. (a, d) Fluorescence, (b, e) darkfield, and (c, f) reflected-light image of a NPs mixture containing four spectrally different types of metallic and alloy-core NPs (Ag@SiO_2+FITC/RBITC, 50/50 Au/Ag@SiO_2+FITC/RBITC) in the presence of fixed retinal cells (ARPE-19) and their respective controls without nanoparticles (d–f).

without any loss of the nanoparticle signal. Moreover, the depth of field for reflected-light microscopy is smaller than that for darkfield, resulting in a better *Z*-axis definition and lower background signal. Colocalization of NPs under three different modes of optical microscopy was possible using fluorescent alloy-core silica-shell nanoparticles as contrast agents (Figure 7). As an additional proof-of-concept experiment, fluorescent Au/Ag@SiO_2 were used for cell-tagging applications by flow cytometry (see Supporting Information). Using a well-known cross-linking chemistry reaction, specific and nonspecific antibodies to HeLa cells were functionalized at the surface of fluorescent core–shell nanoparticles. The results are promising, despite not being perfect, and are paving the way for further improvements in terms of fluorescence intensity because detection specificity was advantageously compared to the use of regular fluorophore-labeled antibodies.

DOI: 10.1021/acs.jpcc.6b11954
J. Phys. Chem. C 2017, 121, 8944–8951

CONCLUSIONS

Fluorescent alloy-core silica-shell nanoparticles were prepared for cell-tagging and -imaging applications. The size and composition of the alloy core can be adjusted to control the position and width of the plasmonics band to meet specific experimental needs. Using a well-known silica-processing reaction, fluorescent silica shells were grown around the alloy nanoparticles, making the nanoparticular architecture well-suited for multiplexed analysis using a multiplatform detection strategy. Retinal cells were observed by fluorescence and darkfield microscopy in the presence of four different color-coded Au/Ag@SiO_2 NPs. Most NPs could be identified by their fluorescence and scattering properties using a simple detection algorithm. On the basis of this proof-of-principle study, it is anticipated to achieve higher levels of multiplexing by better controlling the synthesis of Au/Ag alloy NPs to reduce the width of their size distribution, thus allowing more scattering colors to be used simultaneously without compromising identification capabilities.[40] Furthermore, quantum dots could be incorporated in the silica shell of Au/Ag@SiO_2 NPs instead of fluorophore molecules. A single excitation wavelength would be needed to generate light from all contrast agents, while the narrower emission band of QDs would enhance the multiplexed analysis possibilities of Au/Ag@SiO_2. Finally, the applicability of fluorescent alloy-core silica shell nanoparticles for cell-tagging and -imaging applications was presented. This highly reliable synthesis process offers great control on the size and composition of the final NPs. The latter can be exploited to generate nanostructures with specific photophysical and spectral properties, making this technology highly versatile. The scattering color adjustability of the alloy-core nanoparticles could be exploited in the design of a new cytometry platform with color-coded scattering signal detection capabilities. The principal advantage of scattering over fluorescence is the time stability of the signal over time. Using alloy nanoparticles, one can create a multiplex-labeling assay specifically designed for long time observations using low-light excitation: it is ideal for cell observation because it offers adjustable photophysical properties to suits specific experimental needs, thus representing a cheaper alternative to conventional cell-labelling moieties in terms of detectability and photostability.

ASSOCIATED CONTENT

Supporting Information

The Supporting Information is available free of charge on the ACS Publications website at DOI: 10.1021/acs.jpcc.6b11954.

Fluorescence characterization and MEF factor determination; parameters used for NP absorbance modeling; energy-dispersive X-ray spectroscopy for alloy-core compositional analysis; characterization of NP concentration; NP functionalization with antibodies; cell-preparation and cell-sorting experiments with flow cytometry (PDF)

AUTHOR INFORMATION

Corresponding Authors

*E-mail: danny.brouard@hema-quebec.qc.ca.
*E-mail: michel.meunier@polymtl.ca.

ORCID

Michel Meunier: 0000-0002-2398-5602

Notes

The authors declare no competing financial interest.

ACKNOWLEDGMENTS

This work was supported by the Nature Science and Engineering Research Council of Canada NSERC. The authors would like to thank Jean-Philippe Masse for the help with the TEM and EDS measurements accomplished at the Center for Characterization and Microscopy of Materials (CM^2).

REFERENCES

(1) Chen, J.; Wiley, B.; Li, Z. Y.; Campbell, D.; Saeki, F.; Cang, H.; Au, L.; Lee, J.; Li, X.; Xia, Y. Gold Nanocages: Engineering .Their Structure for Biomedical Applications. *Adv. Mater.* **2005**, *17*, 2255−2261.

(2) Zhu, Y. Y.; Kuang, H.; Xu, L. G.; Ma, W.; Peng, C. F.; Hua, Y. F.; Wang, L. B.; Xu, C. L. Gold Nanorod Assembly Based Approach to Toxin Detection by SERS. *J. Mater. Chem.* **2012**, *22*, 2387−2391.

(3) Willner, I.; Katz, E. Magnetic Control of Electrocatalytic and Bioelectrocatalytic Processes. *Angew. Chem., Int. Ed.* **2003**, *42*, 4576−4588.

(4) Lee, S.; Chon, H.; Lee, M.; Choo, J.; Shin, S. Y.; Lee, Y. H.; Rhyu, I. J.; Son, S. W.; Oh, C. H. Surface-Enhanced Raman Scattering Imaging of HER2 Cancer Markers Overexpressed in Single MCF7 Cells Using Antibody Conjugated Hollow Gold Nanospheres. *Biosens. Bioelectron.* **2009**, *24*, 2260−2263.

(5) Kulkarni, A. P.; Noone, K. M.; Munechika, K.; Guyer, S. R.; Ginger, D. S. Plasmon-Enhanced Charge Carrier Generation in Organic Photovoltaic Films Using Silver Nanoprisms. *Nano Lett.* **2010**, *10*, 1501−1505.

(6) Larson, D. R.; Ow, H.; Vishwasrao, H. D.; Heikal, A. A.; Wiesner, U.; Webb, W. W. Silica Nanoparticle Architecture Determines Radiative Properties of Encapsulated Fluorophores. *Chem. Mater.* **2008**, *20*, 2677−2684.

(7) Tokonami, S.; Yamamoto, Y.; Shiigi, H.; Nagaoka, T. Synthesis and Bioanalytical Applications of Specific-Shaped Metallic Nanostructures: A Review. *Anal. Chim. Acta* **2012**, *716*, 76−91.

(8) Guerrero-Martínez, A.; Pérez-Juste, J.; Liz-Marzán, L. M. Recent Progress on Silica Coating of Nanoparticles and Related Nanomaterials. *Adv. Mater.* **2010**, *22*, 1182−1195.

(9) Seekell, K.; Crow, M. J.; Marinakos, S.; Ostrander, J.; Chilkoti, A.; Wax, A. Hyperspectral Molecular Imaging of Multiple Receptors Using Immunolabeled Plasmonic Nanoparticles. *J. Biomed. Opt.* **2011**, *16*, 116003.

(10) MacLaughlin, C. M.; Mullaithilaga, N.; Yang, G.; Ip, S. Y.; Wang, C.; Walker, G. C. Surface-Enhanced Raman Scattering Dye-Labeled Au Nanoparticles for Triplexed Detection of Leukemia and Lymphoma Cells and SERS Flow Cytometry. *Langmuir* **2013**, *29*, 1908−1919.

(11) Saha, A.; Basiruddin, S. K.; Sarkar, R.; Pradhan, N.; Jana, N. R. Functionalized Plasmonic-Fluorescent Nanoparticles for Imaging and Detection. *J. Phys. Chem. C* **2009**, *113*, 18492−18498.

(12) Patskovsky, S.; Bergeron, E.; Rioux, D.; Simard, M.; Meunier, M. Hyperspectral Reflected Light Microscopy of Plasmonic Au/Ag Alloy Nanoparticles Incubated as Multiplex Chromatic Biomarkers with Cancer Cells. *Analyst* **2014**, *139*, 5247−5253.

(13) Lachaine, R.; Boutopoulos, C.; Lajoie, P. Y.; Boulais, É.; Meunier, M. Rational Design of Plasmonic Nanoparticles for Enhanced Cavitation and Cell Perforation. *Nano Lett.* **2016**, *16*, 3187−3194.

(14) Spivakov, M.; Fisher, A. G. Epigenetic Signatures of Stem-Cell Identity. *Nat. Rev. Genet.* **2007**, *8*, 263−271.

(15) Steward, R. L.; Cheng, C. M.; Wang, D. L.; LeDuc, P. R. Probing Cell Structure Responses Through a Shear and Stretching Mechanical Stimulation Technique. *Cell Biochem. Biophys.* **2010**, *56*, 115−124.

(16) Tennant, J. R. Evaluation of the Trypan Blue Technique for Determination of Cell Viability. *Transplantation* **1964**, *2*, 685.

DOI: 10.1021/acs.jpcc.6b11954
J. Phys. Chem. C 2017, 121, 8944−8951

(17) Cunningham, A. J.; Szenberg, A. Further Improvements in the Plaque Technique for Detecting Single Antibody-Forming Cells. *Immunology* **1968**, *14*, 599−600.
(18) Krichevsky, O.; Bonnet, G. Fluorescence Correlation Spectroscopy: The Technique and Its Applications. *Rep. Prog. Phys.* **2002**, *65*, 251−297.
(19) Singh, N. P.; McCoy, M. T.; Tice, R. R.; Schneider, E. L. A Simple Technique for Quantitation of Low Levels of DNA Damage in Individual Cells. *Exp. Cell Res.* **1988**, *175*, 184−191.
(20) Nicoletti, I.; Migliorati, G.; Pagliacci, M. C.; Grignani, F.; Riccardi, C. A Rapid and Simple Method for Measuring Thymocyte Apoptosis by Propidium Iodide Staining and Flow Cytometry. *J. Immunol. Methods* **1991**, *139*, 271−279.
(21) Bergeron, É.; Patskovsky, S.; Rioux, D.; Meunier, M. 3D Multiplexed Immunoplasmonics Microscopy. *Nanoscale* **2016**, *8*, 13263−13272.
(22) te Velde, E. A.; Veerman, T.; Subramaniam, V.; Ruers, T. The Use of Fluorescent Dyes and Probes in Surgical Oncology. *Eur. J. Surg. Oncol.* **2010**, *36*, 6−15.
(23) Yu, C.; Nakshatri, H.; Irudayaraj, J. Identity Profiling of Cell Surface Markers by Multiplex Gold Nanorod Probes. *Nano Lett.* **2007**, *7*, 2300−2306.
(24) Lee-Montiel, F. T.; Li, P.; Imoukhuede, P. I. Quantum Dot Multiplexing for the Profiling of Cellular Receptors. *Nanoscale* **2015**, *7*, 18504−18514.
(25) Bruchez, M., Jr. Semiconductor Nanocrystals as Fluorescent Biological Labels. *Science* **1998**, *281*, 2013−2016.
(26) Wegner, K. D.; Hildebrandt, N. Quantum Dots: Bright and Versatile in Vitro and in Vivo Fluorescence Imaging Biosensors. *Chem. Soc. Rev.* **2015**, *44*, 4792−4834.
(27) El-Sayed, I. I. H.; Huang, X.; El-Sayed, M. A. M. Surface Plasmon Resonance Scattering and Absorption of Anti-EGFR Antibody Conjugated Gold Nanoparticles in Cancer Diagnostics: Applications in Oral Cancer. *Nano Lett.* **2005**, *5*, 829−834.
(28) Ghosh, P.; Han, G.; De, M.; Kim, C. K.; Rotello, V. M. Gold Nanoparticles in Delivery Applications. *Adv. Drug Delivery Rev.* **2008**, *60*, 1307−1315.
(29) Ahamed, M.; AlSalhi, M. S.; Siddiqui, M. K. J. Silver Nanoparticle Applications and Human Health. *Clin. Chim. Acta* **2010**, *411*, 1841−1848.
(30) Kim, D.; Park, S.; Lee, J. H.; Jeong, Y. Y.; Jon, S. *J. Am. Chem. Soc.* **2007**, *129*, 7661−7665.
(31) Wang, Y.; Xie, X.; Wang, X.; Ku, G.; Gill, K. L.; O'Neal, D. P.; Stoica, G.; Wang, L. V. Photoacoustic Tomography of a Nanoshell Contrast Agent in the in Vivo Rat Brain. *Nano Lett.* **2004**, *4*, 1689−1692.
(32) Na, H. B.; Lee, J. H.; An, K.; Park, Y. Il; Park, M.; Lee, I. S.; Nam, D.-H.; Kim, S. T.; Kim, S.-H.; Kim, S.-W.; et al. [21b]-Development of aT1 Contrast Agent for Magnetic Resonance Imaging Using MnO Nanoparticles. *Angew. Chem., Int. Ed.* **2007**, *46*, 5397−5401.
(33) Aslan, K.; Wu, M.; Lakowicz, J. R.; Geddes, C. D. Fluorescent Core-Shell Ag@SiO2 Nanocomposites for Metal-Enhanced Fluorescence and Single Nanoparticle Sensing Platforms. *J. Am. Chem. Soc.* **2007**, *129*, 1524−1525.
(34) Viger, M. L.; Live, L. S.; Therrien, O. D.; Boudreau, D. Reduction of Self-Quenching in Fluorescent Silica-Coated Silver Nnanoparticles. *Plasmonics* **2008**, *3*, 33−40.
(35) Liu, S. H.; Han, M. Y. Synthesis, Functionalization, and Bioconjugation of Monodisperse, Silica-Coated Gold Nanoparticles: Robust Bioprobes. *Adv. Funct. Mater.* **2005**, *15*, 961−967.
(36) Hu, R.; Yong, K. T.; Roy, I.; Ding, H.; He, S.; Prasad, P. N. Metallic Nanostructures as Localized Plasmon Resonance Enhanced Scattering Probes for Multiplex Dark-Field Targeted Imaging of Cancer Cells. *J. Phys. Chem. C* **2009**, *113*, 2676−2684.
(37) Von Maltzahn, G.; Centrone, A.; Park, J. H.; Ramanathan, R.; Sailor, M. J.; Hatton, T. A.; Bhatia, S. N. SERS-Coded Cold Nanorods as a Multifunctional Platform for Densely Multiplexed near-Infrared Imaging and Photothermal Heating. *Adv. Mater.* **2009**, *21*, 3175−3180.
(38) Liz-Marzán, L. M. Tailoring Surface Plasmons Through the Morphology and Assembly of Metal Nanoparticles. *Langmuir* **2006**, *22*, 32−41.
(39) Burda, C.; Chen, X.; Narayanan, R.; El-Sayed, M. A. Chemistry and Properties of Nanocrystals of Different Shapes. *Chem. Rev.* **2005**, *105*, 1025−1102.
(40) Rioux, D.; Meunier, M. Seeded Growth Synthesis of Composition and Size-Controlled Gold−Silver Alloy Nanoparticles. *J. Phys. Chem. C* **2015**, *119*, 13160−13168.
(41) Lakowicz, J. R.; Malicka, J.; D'Auria, S.; Gryczynski, I. Release of the Self-Quenching of Fluorescence Near Silver Metallic Surfaces. *Anal. Biochem.* **2003**, *320*, 13−20.
(42) Lessard-Viger, M.; Rioux, M.; Rainville, L.; Boudreau, D. FRET Enhancement in Multilayer Core-Shell Nanoparticles. *Nano Lett.* **2009**, *9*, 3066−3071.
(43) Eustis, S.; el-Sayed, M. A. Why Gold Nanoparticles Are More Precious than Pretty Gold: Noble Metal Surface Plasmon Resonance and Its Enhancement of the Radiative and Nonradiative Properties of Nanocrystals of Different Shapes. *Chem. Soc. Rev.* **2006**, *35*, 209−217.
(44) Dondapati, S. K.; Sau, T. K.; Hrelescu, C.; Klar, T. A.; Stefani, F. D.; Feldmann, J. Label-Free Biosensing Based on Single Gold Nanostars as Plasmonic Transducers. *ACS Nano* **2010**, *4*, 6318−6322.
(45) Tovmachenko, O. G.; Graf, C.; Van Den Heuvel, D. J.; Van Blaaderen, A.; Gerritsen, H. C. Fluorescence Enhancement by Metal-Core/silica-Shell Nanoparticles. *Adv. Mater.* **2006**, *18*, 91−95.
(46) Brouard, D.; Viger, M. L.; Bracamonte, A. G.; Boudreau, D. Label-Free Biosensing Based on Multilayer Fluorescent Nanocomposites and a Cationic Polymeric Transducer. *ACS Nano* **2011**, *5*, 1888−1896.
(47) Cheng, D.; Xu, Q.-H. Separation Distance Dependent Fluorescence Enhancement of Fluorescein Isothiocyanate by Silver Nanoparticles. *Chem. Commun. (Cambridge, U. K.)* **2007**, 248−250.
(48) Liz-marzan, L. M.; Giersig, M.; Mulvaney, P. Synthesis of Nanosized Gold−Silica Core−Shell Particles. *Langmuir* **1996**, *12*, 4329−4335.
(49) Zhang, Y.; Kong, X.; Xue, B.; Zeng, Q.; Liu, X.; Tu, L.; Liu, K.; Zhang, H. A Versatile Synthesis Route for metal@SiO2 Core−shell Nanoparticles Using 11-Mercaptoundecanoic Acid as Primer. *J. Mater. Chem. C* **2013**, *1*, 6355.
(50) Ung, T.; Liz-marzan, L. M.; Mulvaney, P. Controlled Method for Silica Coating of Silver Colloids. Influence of Coating on the Rate of Chemical Reactions. *Langmuir* **1998**, *14*, 3740−3748.
(51) Rodríguez-González, B.; Sánchez-Iglesias, A.; Giersig, M.; Liz-Marzán, L. M. AuAg Bimetallic Nanoparticles: Formation, Silica-Coating and Selective Etching. *Faraday Discuss.* **2004**, *125*, 133−144 and discussion on pp 195−219..
(52) Lachaine, R.; Boulais, É.; Rioux, D.; Boutopoulos, C.; Meunier, M. Computational Design of Durable Spherical Nanoparticles with Optimal Material, Shape, and Size for Ultrafast Plasmon-Enhanced Nanocavitation. *ACS Photonics* **2016**, *3*, 2158−2169.
(53) Rioux, D.; Vallières, S.; Besner, S.; Muñoz, P.; Mazur, E.; Meunier, M. An Analytic Model for the Dielectric Function of Au, Ag, and Their Alloys. *Adv. Opt. Mater.* **2014**, *2*, 176−182.
(54) Malitson, I. H. Interspecimen Comparison of the Refractive Index of Fused Silica. *J. Opt. Soc. Am.* **1965**, *55*, 1205.
(55) Mie, G. Beiträge Zur Optik Trüber Medien, Speziell Kolloidaler Metallösungen. *Ann. Phys.* **1908**, *330*, 377−445.
(56) Li, Z.; Jia, L.; Li, Y.; He, T.; Li, X.-M. Ammonia-Free Preparation of Ag@SiO2 Core/shell Nanoparticles. *Appl. Surf. Sci.* **2015**, *345*, 122−126.
(57) Fort, E.; Grésillon, S. Surface Enhanced Fluorescence. *J. Phys. D: Appl. Phys.* **2008**, *41*, 013001.
(58) Asselin, J.; Roy, C.; Boudreau, D.; Messaddeq, Y.; Bouchareb, R.; Mathieu, P. Supported Core−shell Nanobiosensors for Quantitative Fluorescence Imaging of Extracellular pH. *Chem. Commun.* **2014**, *50*, 13746−13749.

DOI: 10.1021/acs.jpcc.6b11954
J. Phys. Chem. C 2017, 121, 8944−8951